0026-895X/09/7505-1137–1148$20.00
MOLECULAR PHARMACOLOGY
Copyright © 2009 The American Society for Pharmacology and Experimental Therapeutics
Mol Pharmacol 75:1137–1148, 2009

Vol. 75, No. 5
54494/3466444
Printed in U.S.A.

Nicotine Normalizes Intracellular Subunit Stoichiometry of Nicotinic Receptors Carrying Mutations Linked to Autosomal Dominant Nocturnal Frontal Lobe Epilepsy[S]

Cagdas D. Son, Fraser J. Moss, Bruce N. Cohen, and Henry A. Lester

Division of Biology, California Institute of Technology, Pasadena, California

Received January 2, 2009; accepted February 23, 2009

ABSTRACT

Autosomal dominant nocturnal frontal lobe epilepsy (ADNFLE) is linked with high penetrance to several distinct nicotinic receptor (nAChR) mutations. We studied $(\alpha4)_3(\beta2)_2$ versus $(\alpha4)_2(\beta2)_3$ subunit stoichiometry for five channel-lining M2 domain mutations: S247F, S252L, 776ins3 in $\alpha4$, V287L, and V287M in $\beta2$. $\alpha4$ and $\beta2$ subunits were constructed with all possible combinations of mutant and wild-type (WT) M2 regions, of cyan and yellow fluorescent protein, and of fluorescent and nonfluorescent M3-M4 loops. Sixteen fluorescent subunit combinations were expressed in N2a cells. Förster resonance energy transfer (FRET) was analyzed by donor recovery after acceptor photobleaching and by pixel-by-pixel sensitized emission, with confirmation by fluorescence intensity ratios. Because FRET efficiency is much greater for adjacent than for nonadjacent subunits and the $\alpha4$ and $\beta2$ subunits occupy specific positions in nAChR pentamers, observed FRET efficiencies from $(\alpha4)_3(\beta2)_2$ carrying fluorescent $\alpha4$ subunits were significantly higher than for $(\alpha4)_2(\beta2)_3$; the converse was found for fluorescent $\beta2$ subunits. All tested ADNFLE mutants produced 10 to 20% increments in the percentage of intracellular $(\alpha4)_3(\beta2)_2$ receptors compared with WT subunits. In contrast, 24- to 48-h nicotine (1 μM) exposure increased the proportion of $(\alpha4)_2(\beta2)_3$ in WT receptors and also returned subunit stoichiometry to WT levels for $\alpha4$S248F and $\beta2$V287L nAChRs. These observations may be relevant to the decreased seizure frequency in patients with ADNFLE who use tobacco products or nicotine patches. Fluorescence-based investigations of nAChR subunit stoichiometry may provide efficient drug discovery methods for nicotine addiction or for other disorders that result from dysregulated nAChRs.

Nocturnal frontal lobe epilepsy (NFLE) is marked by seizures that include rhythmic and repetitive limb movements, rapid uncoordinated movements, dystonic posturing, complex motor activities such as sleep walking and pelvic thrusting, and the elevation of the trunk and head with ictal fear and vocalization. NFLE seizures occur primarily during phase 2 of non–rapid-eye-movement sleep. They rarely progress to tonic-clonic convulsions or status epilepticus. There are often uncertain distinctions between NFLE and paroxysmal sleep disorders. The "frontal" description arises from ictal electroencephalographic data, where available, and seizure semiology origin (Provini et al., 1999; Herman et al., 2001; Combi et al., 2004; Derry et al., 2006; Ryvlin et al., 2006).

Autosomal dominant NFLE (ADNFLE) (Scheffer et al., 1995) is linked, with high penetrance, to at least six distinct nAChR mutations in $\alpha4\beta2$ neuronal nicotinic acetylcholine receptors (nAChRs) (Steinlein et al., 1997; Oldani et al., 1998; Combi et al., 2004; Wimmer et al., 2009). Three mutations are in the channel-lining M2 domain of the $\alpha4$ subunit (S247F = S6′F in the commonly used M2 domain renumbering for Cys-loop receptors, S252L = S10′L, and 776ins3, after the 17′ position), whereas two mutations occur in the M2 domain of the $\beta2$ subunit (V287L and V287M at the 22′ position). How the ADNFLE-linked mutations cause seizures, the epileptic focus of ADNFLE seizures, and other basic pathophysiological aspects remain unresolved.

Simple loss of $\alpha4\beta2$ receptor function does not seem to cause ADNFLE. Knockout mice with genetic deletions of the $\alpha4$ or $\beta2$ subunit do not display spontaneous seizures or any

This work was supported by the National Institutes of Health National Institute of Neurological Disorders and Stroke [Grant NS11756]; by Targacept, Inc.; by a fellowship from Philip Morris USA/International (to C.D.G.); and by a fellowship from the American Heart Association (to F.J.M.).

Article, publication date, and citation information can be found at http://molpharm.aspetjournals.org.

doi:10.1124/mol.108.054494.

[S] The online version of this article (available at http://molpharm.aspetjournals.org) contains supplemental material.

ABBREVIATIONS: NFLE, nocturnal frontal lobe epilepsy; ADNFLE, autosomal dominant nocturnal frontal lobe epilepsy; nAChR, nicotinic acetylcholine receptor; ACh, acetylcholine; CFP, cyan fluorescent protein; YFP, yellow fluorescent protein; XFP, cyan or yellow fluorescent protein; FRET, Förster resonance energy transfer; DRAP, donor recovery after acceptor photobleaching; FIR, fluorescence intensity ratio; FBS, fetal bovine serum; DMEM, Dulbecco's modified Eagle's medium; SBT, spectral bleedthrough; WT, wild type.

nicotine-induced phenotype resembling ADNFLE seizures (Wong et al., 2002; Teper et al., 2007; M. Picciotto, Yale School of Medicine, New Haven, CT, personal communication). One hypothesis suggests that ADNFLE mutations initiate seizures by increasing the sensitivity of $\alpha4\beta2$ nicotinic receptors to the endogenous agonist acetylcholine (ACh) (Bertrand et al., 2002). Our own work (Figl et al., 1998; Rodrigues-Pinguet et al., 2003; Rodrigues-Pinguet et al., 2005) and that of others (Steinlein et al., 1997) shows that reduced allosteric Ca^{2+} potentiation of the $\alpha4\beta2$ ACh response is another common feature of ADNFLE mutations.

A more subtle pathophysiological suggestion arises from the observations that $\alpha4\beta2$ nAChRs exist at least in two different stoichiometries. Although the stoichiometry of human $\alpha4\beta2$ nAChRs in neurons has not yet been elucidated, in mouse brain preparations there are biphasic agonist concentration-response curves for stimulation of putative $\alpha4\beta2$ nAChR function (Fonck et al., 2003, 2005). Likewise, $\alpha4$ and $\beta2$ nAChR subunits that are expressed heterologously in mammalian cell lines (Nelson et al., 2003; Kuryatov et al., 2005; Vallejo et al., 2005) or *Xenopus laevis* oocytes (Zwart et al., 2006) assemble into a mixture of receptors with two distinct agonist sensitivities. The dominant stoichiometry in these heterologous systems is often the low-sensitivity $(\alpha4)_3(\beta2)_2$ nAChR (Nelson et al., 2003; Kuryatov et al., 2005; Moroni et al., 2006). Most investigations of heterologously expressed ADNFLE mutants reveal left-shifted dose-response relations, so it has been natural to suspect that this arises from altered subunit stoichiometry.

Nicotine and tobacco use decreases the frequency of ADNFLE seizures (Willoughby et al., 2003; Brodtkorb and Picard, 2006). $\alpha4\beta2$ receptors may be the primary nAChR subtype affected by nicotine concentrations (100–500 nM) found in the blood of smokers (Benowitz et al., 1982). Long-term exposure to nicotine initiates a cascade of events, such as activation and desensitization of nAChRs, induction of long-term potentiation, and depression at glutamatergic synapses (Mansvelder and McGehee, 2000; Partridge et al., 2002), behavioral tolerance, dependence, and withdrawal. Long-term exposure to nicotine also causes a shift in nAChR subunit stoichiometry in heterologous expression systems (Nelson et al., 2003). To understand whether the nAChR subunit stoichiometry is altered in ADNFLE, and how nicotine might have an effect on seizure suppression, we analyzed the effects of each mutation on $\alpha4\beta2$ nAChR subunit stoichiometry. We also analyzed effects of nicotine. The primary tools were Förster resonance energy transfer (FRET) and fluorescence intensity ratios (FIR).

Materials and Methods

Materials. pEYFP-C1 and pECFP-C1 vectors were purchased from Clontech (Mountain View, CA). PfuTurbo C_x Hotstart polymerase and the QuikChange II XL site-directed mutagenesis kit were purchased from Stratagene (La Jolla, CA). The mouse neuroblastoma 2a (N2a; CCL-131) was obtained from American Type Culture Collection (Manassas, VA). The pcDNA3.1(+) expression vector, fetal bovine serum, Lipofectamine and Plus reagents were purchased from Invitrogen (Carlsbad, CA). Penicillin/streptomycin (100×) and sodium pyruvate (100×) solutions were purchased from Mediatech (Herndon, VA). Culture dishes (35 mm, with no. 0 thickness 14-mm 0 glass coverslip microwells) were purchased from Mattek (Ashland, MA). Other tissue-culture plasticware was purchased from Greiner Bio-One (Monroe, CA). ACh, nicotine, and all other reagents were purchased from SigmaAldrich (St. Louis, MO).

Molecular Biology. Wild-type (WT) mouse $\alpha4$ and $\beta2$ nAChR cDNAs were kindly provided by Jerry Stitzel (University of Michigan, Ann Arbor, MI) and the construction of fluorescent $\alpha4$YFP, $\alpha4$CFP, $\beta2$YFP, and $\beta2$CFP nAChR subunits has been described previously (Nashmi et al., 2003). Fluorescent ADNFLE mutants were generated in QuikChange II XL mutagenesis PCR reactions from the WT $\alpha4$ and $\beta2$ fluorescent subunits ($\alpha4$XFP and $\beta2$XFP) plasmids using the primer pairs described in Supplementary Table 1. For each construct, the entire open reading frame and its flanking regions were sequenced.

Cell Culture and Transfections. N2a cells were cultured at 37°C in 95% air/5% CO_2 in medium composed of 44.5% DMEM, 44.5% Opti-MEM 1, 5% fetal bovine serum, 100 IU/ml penicillin, and 100 μg/ml streptomycin. For all experiments, cells were plated onto poly-*d*-lysine-coated 35-mm culture dishes with 14-mm glass bottoms. Transfections were performed using a modification of the manufacturer's Lipofectamine and Plus reagent protocol, resulting in nonsaturated expression levels of nAChRs (Imoukhuede et al., 2009). cDNA was diluted in DMEM in one tube to which Plus reagent was subsequently added. The total cDNA in each transfection mix was always 1 μg, and the proportion of $\alpha4$ and $\beta2$ cDNAs used in each experiment are stated in the relevant results section. In a second tube, Lipofectamine was diluted in DMEM. The tubes were briefly vortexed and incubated at room temperature for 15 min. The diluted Lipofectamine was subsequently added to the cDNA/Plus reagent dilution and vortexed. The transfection mixes were incubated for a further 15 min at room temperature, whereas the preplated cells were washed once with DMEM to remove residual serum from the culture media, and then 800 μl of DMEM added to perform the transfection. Sixteen hours after the cells were originally plated, the cDNA/Plus/Lipofectamine mixes (200 μl) were added to the dishes. The transfections were incubated at 37°C for 3 h; then, 2.5 ml of N2a medium was added. Nicotine at 1 μM final concentration was added to the appropriate dishes (nicotine was replenished with each change of medium). After 16 h the transfection cocktail was replaced by complete N2a medium and again 24 h later.

Confocal Imaging. Live cells grown on 14-mm glass-bottomed Mattek 35-mm culture dishes precoated with poly-*d*-lysine were washed twice with 37°C, pH 7.4, extracellular buffer (150 mM NaCl, 4 mM KCl, 10 mM HEPES, 2 mM $MgCl_2$, 2 mM $CaCl_2$, and 10 mM glucose) and observed in the same solution. Imaging was performed at room temperature on an Eclipse C1si laser-scanning confocal microscope equipped with a 63×, 1.4 numerical aperture, violet-corrected plan apochromatic oil objective and a multianode photomultiplier tube with 32 channels (Nikon Instruments Inc., Melville, NY). Where required, images were linearly unmixed with the EZ-C1 software (Nikon) for the emission spectra of the fluorophores of interest using reference spectra individually compiled for each fluorophore expressed in the same cell type and imaged under identical experimental conditions. Quantification of images was performed using ImageJ version 1.41g (http://rsb.info.nih.gov/ij/).

Donor Recovery after Acceptor Photobleach FRET. N2a cells were visualized at room temperature in extracellular buffer, 48 h after transfection. A series of lambda stack X-Y images were collected with the Eclipse C1si laser-scanning confocal microscope. Dequenching of CFP fluorescence during incremental photobleaching of YFP was performed and analyzed as described previously (Nashmi et al., 2003; Drenan et al., 2008). FRET efficiency (E) was calculated:

$$E = 1 - \left(\frac{I_{DA}}{I_D}\right) \quad (1)$$

I_{DA} represents the normalized fluorescence intensity of CFP (100%) in the presence of nonbleached acceptor. I_D represents the normalized fluorescence intensity of CFP after 100% photobleach of

the acceptor YFP. The I_D value was extrapolated from a scatter plot of the percentage increase of CFP versus the percentage decrease of YFP for each cell (Nashmi et al., 2003). This method of determining FRET is used for the data in Figs. 2 to 4.

Pixel-by-Pixel FRET from Sensitized Acceptor Emission. Full emission spectra were acquired in 5-nm bins between 450 and 610 nm and linearly unmixed using reference spectra from samples expressing solely the CFP- or YFP-fusion constructs to separate the CFP and YFP signals from each pixel of the spectral images. Transfections of cells expressing only the CFP- or YFP-fusion protein were performed for every imaging session to control for pixel saturation and spectral bleedthrough (SBT). Where appropriate, nonfluorescent subunit cDNAs were included in the transfection to ensure the faithful expression and subcellular localization of the single fluorescent species. Control samples expressing only the CFP-fusion constructs were imaged with the 439.5-nm laser line and unmixed with YFP and CFP spectra. The unmixed YFP images were termed the $FRET_C$ channel, and the fluorescence intensity of each pixel was termed (I_{FRETC}). The CFP images were the "Donor" channel, and pixel intensities were described by I_{CFP}. A montage of all the $FRET_C$ channel images, and a second montage of all the Donor channel images were assembled and compiled into an image stack called the "Donor SBT stack" in the order $FRET_C$ channel, Donor channel. Two spectral images of each cell expressing only the YFP fusion constructs were acquired, the first excited by the laser line at 439.5 nm and the second at 514 nm. The YFP signal was unmixed from each image. A montage of the unmixed YFP images excited at 439.5 nm, termed the $FRET_Y$ channel (pixel intensities = I_{FRETY}), was assembled and compiled with a montage of the YFP images excited at 514 nm, termed the Acceptor channel (pixel intensities = I_{YFP}), and called the Acceptor SBT image stack.

The Donor and Acceptor SBT stacks were processed by the PixFRET ImageJ plugin to assess the CFP and YFP bleedthroughs (Feige et al., 2005). The donor SBT ratio (I_{FRETC}/I_{CFP}) was plotted as a function of I_{CFP} to model the CFP SBT (BT_{CFP}) for each pixel in the FRET images. The acceptor SBT ratio (I_{FRETY}/I_{YFP}) was plotted as a function of I_{YFP} to model the YFP bleedthrough (BT_{YFP}) for each pixel in the FRET images. If linear, the best fit of the bleedthrough plot gave the constants a_{XFP} and b_{XFP} in the equation $BT_{XFP} = a_{XFP} \cdot I_{XFP} + b_{XFP}$ (where XFP is either the donor or the acceptor fluorophore). If an exponential, the best fit of the bleedthrough plot gave the constants c_{XFP}, d_{XFP}, and e_{XFP} in the equation $BT_{XFP} = c_{XFP}\, exp\,(I_{XFP} \cdot d_{XFP}) + e_{XFP}$.

Unmixed images for each cell were compiled into stacks of three 16-bit images in the channel order FRET, Donor, and Acceptor. From this stack a region of interest was selected to determine the background intensity for all three images in the stack. With the background and SBT corrections set, the net FRET (nF) for each pixel was calculated, and the data were output as a 32-bit image:

$$nF = I_{FRET} - I_{CFP}BT_{CFP} - I_{YFP}BT_{YFP}. \quad (2)$$

FRET efficiency could not be directly determined by eq. 1 from sensitized emission experiments because it is not possible to measure I_D directly from such samples. However, because the sensitized emission of the acceptor is due to the quenching of the donor in the presence of the acceptor, I_D can be determined (Elangovan et al., 2003) by adding the nF signal intensity to the intensity of the donor in the presence of acceptor I_{DA}. Substituting $I_D = I_{DA} + nF$ into eq. 1, one has:

$$E = 1 - \left(\frac{I_{DA}}{I_{DA} + nF}\right), \quad (3)$$

This method for measuring FRET is employed for the data in Figs. 5 and 6.

Results

FRET Efficiencies Reflect Stoichiometry. The calculations and analyses presented in the *Appendix* and summarized by Fig. 1 show that when 1) only the $\alpha4$ subunits are fluorescently tagged with a 1:1 M ratio of CFP and YFP, and 2) the $(\alpha4)_3(\beta2)_2$ receptor stoichiometry predominates, one expects robust FRET. Upon a shift toward the $(\alpha4)_2(\beta2)_3$ stoichiometry, one expects a lower FRET efficiency. These expected differences in FRET arise because, in a pentamer containing three $\alpha4$ subunits, two are adjacent. Because the FRET efficiency approaches a $1/R^6$ dependence as fluorophores are separated, our assumptions predict a much higher FRET efficiency in this case. Likewise, 1) when only the $\beta2$ subunits are fluorescently tagged with a 1:1 M ratio of CFP and YFP, and 2) when the $(\alpha4)_2(\beta2)_3$ receptor stoichiometry predominates, one expects a higher FRET efficiency.

Cells often produce a mixture of these $(\alpha4)_2(\beta2)_3$ and $(\alpha4)_3(\beta2)_2$ receptors (Buisson and Bertrand, 2001; Nashmi et al., 2003; Nelson et al., 2003), although they can be manipulated to express a nearly pure population of one or the other (Nelson et al., 2003; Briggs et al., 2006). We have optimized an N2a cell expression system to produce controlled, nonsaturated expression of membrane proteins, suitable for fluorescence studies (Drenan et al., 2008; Imoukhuede et al., 2009). We transfected N2a cells with various ratios of subunit cDNA, to force the receptor population toward a mostly $(\alpha4)_3(\beta2)_2$ or $(\alpha4)_2(\beta2)_3$ stoichiometry (Nelson et al., 2003). As typically found for nAChRs, there was little membrane-localized fluorescence at the cell periphery in any of the images of this study; therefore most of the fluorescence arises from intracellular receptors.

To study FRET, we intentionally bleached the YFP fluorophore while monitoring fluorescence from both the YFP and CFP fluorophores. Changes in fluorescence intensity versus time were plotted (Fig. 2B), and FRET efficiency was calculated as described under *Materials and Methods* (Fig. 2, C–E). Measured FRET efficiencies ranged from 5 to 18% for various transfections with forced stoichiometries. As expected, we observed a monotonic increase in FRET when the fluorophores were attached to the $\alpha4$ subunit and the mole fraction of $\alpha4$ cDNA was increased, shifting the stoichiometry toward $(\alpha4)_3(\beta2)_2$ (Fig. 2D). Likewise, higher FRET efficiencies were observed when the fluorophores are attached to the $\beta2$ subunit and the stoichiometry was shifted toward $(\alpha4)_2(\beta2)_3$ population.

We correlated these measurements with the calculated values, assuming 52 Å as the shortest distance a between two fluorophores, using the linear relation summarized in Fig. 1D. Results showed that when the N2a cells are transfected with 4:1 cDNA ratio of $\alpha4$:$\beta2$, ~90% of the assembled receptors have the $(\alpha4)_3(\beta2)_2$ stoichiometry. Increasing the mole fraction of the $\beta2$ cDNA in the transfection mixture increased the $(\alpha4)_2(\beta2)_3$ form, as expected. Interestingly, transfection with 1:1 cDNA ratio resulted in 60 to 70% $(\alpha4)_3(\beta2)_2$; similar results were previously reported using biochemical assays (Nelson et al., 2003). It is noteworthy that these results are also confirmed by an independent series of measurements that use FIR (Supplementary Fig. 1). These results confirmed that qualitatively, and to some extent quantitatively, higher FRET is observed when there are three rather than

two fluorophore-labeled subunits of a single subtype in $(\alpha4)_n(\beta2)_{5-n}$ receptors.

ADNFLE Mutations Bias Stoichiometry Toward $(\alpha4)_3(\beta2)_2$: Donor Recovery after Acceptor Photobleach Assays. In one set of experiments, we analyzed donor recovery after acceptor photobleach (DRAP) FRET efficiency values from N2a cells transfected with nonfluorescent ADNFLE mutants plus fluorescently tagged complementary WT subunits (Fig. 3, A and B). There were two subsets of these experiments. One used $\alpha4$ ADNFLE subunits plus fluorescent $\beta2$ subunits (denoted $\beta2$XFP in Fig. 3, A and B); the other used $\beta2$ ADNFLE subunits plus fluorescent $\alpha4$ subunits (denoted $\alpha4$XFP in Fig. 3, A and B). We carried out 1:4 (Fig. 3A) and 1:1 cDNA (Fig. 3B) transfection ratios for the two nAChR subunits $\alpha4$ and $\beta2$, respectively. (We chose the 1:4 ratio because, as shown below, the ADNFLE mutations seem to favor nAChRs containing more $\alpha4$ than $\beta2$ subunits, and it was important to know whether merely changing the cDNA ratios could reverse this effect). In nearly all cases, FRET values differed significantly from the values for the corresponding fluorescently labeled WT subunits. The $\alpha4$ mutants tested (776ins3, S248F, and S252L) showed significantly lower FRET efficiencies compared with the $\alpha4\beta2$XFP control. This decrease in FRET efficiency suggested an increased $(\alpha4)_3(\beta2)_2$ receptor population versus the WT subunits. On the other hand, the two $\beta2$ subunit ADNFLE mutants showed a significant increase in FRET efficiency compared with the $\alpha4$XFP$\beta2$ control. These results also suggest an increased $(\alpha4)_3(\beta2)_2$ receptor population versus the control cells. All five of the 1:4 cDNA transfection pairs (Fig. 3A), and all five of the 1:1 cDNA transfection pairs (Fig. 3B) displayed a significant shift in subunit stoichiometry toward the $(\alpha4)_3(\beta2)_2$ configuration.

In a second set of experiments, we analyzed FRET efficiency values from N2a cells transfected with subunits that contained both ADNFLE mutations and XFP labels (Fig. 3, C and D). The complementary subunits were WT. These experiments were performed with the five M2 domain ADNFLE mutations studied in the experiments described above. Again, there were two subsets of these experiments. One used $\alpha4$ ADNFLE fluorescent subunits (Fig. 3, C and D) plus nonfluorescent $\beta2$ subunits; the other used $\beta2$ ADNFLE fluorescent subunits (Fig. 3, C and D) plus nonfluorescent $\alpha4$ subunits. We carried out 1:4 cDNA (Fig. 3C) and 1:1 cDNA (Fig. 3D) transfection ratios for the $\alpha4$ and $\beta2$ subunits, respectively. In four of five cases for both transfection ratios, the change in the FRET efficiency indicated a shift toward the $(\alpha4)_3(\beta2)_2$ receptor population.

This set of DRAP FRET experiments shows that, under 18 of 20 conditions, the ADNFLE mutations significantly ($p < 0.05$) shift the stoichiometry of $\alpha4\beta2$ receptor population toward the $(\alpha4)_3(\beta2)_2$ stoichiometry. This major result is

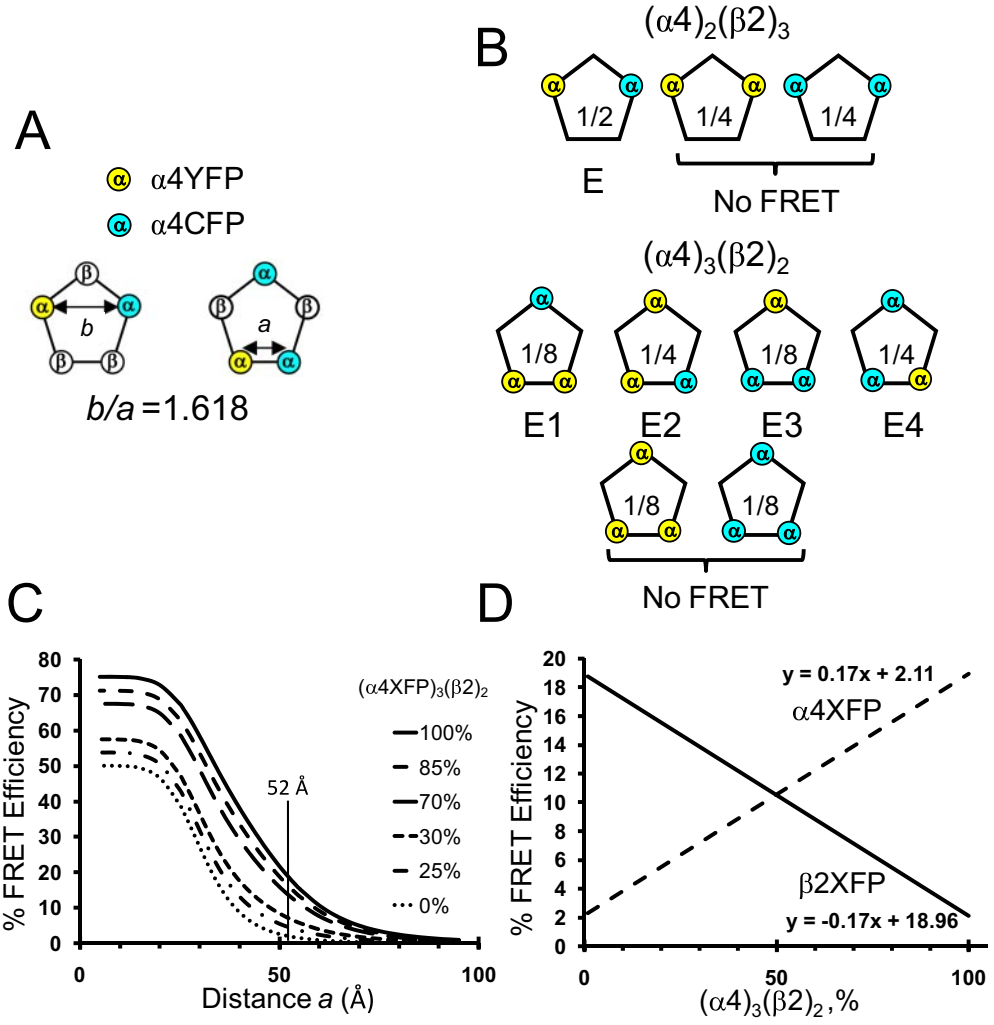

Fig. 1. Assumptions and calculations underlying the FRET analyses. A, in a pentamer, there are two possible distances between fluorophores: "*a*," the side length of the pentagon, and "*b*," the diagonal between nonadjacent subunits. See *Appendix*, eq. 4. B, fractional prevalence of various arrangements when two or three tagged subunits are present in pentameric nAChRs. FRET efficiencies *E*, *E*1, *E*2, *E*3, and *E*4 are given in *Appendix*, eqs. 5 to 9 (Corry et al., 2005). C, theoretical FRET efficiency versus distance *a* between adjacent fluorophores in $\alpha4$ subunits, for $\alpha4\beta2$ receptor populations containing several overall stoichiometric ratios of $\alpha4$ to $\beta2$. Calculations use *Appendix* eqs. 7 to 10 plus the known statistical factors (Corry et al., 2005). For the CFP-YFP pair, the Förster distance, $R_0 = 50$ Å. Note that *x*-axis is defined by the length of a side rather than the definition given by Figs. 10 and 12 of Corry et al. (2005). D, dashed line, calculated FRET efficiency for fluorescent $\alpha4$ subunits, versus percentage of receptors with $(\alpha4)_3(\beta2)_2$ stoichiometry (the balance of pentamers would be $(\alpha4)_2(\beta2)_3$). The solid line provides the complementary calculation for receptors with fluorescent $\beta2$ subunits. The calculations assume that the separation between adjacent fluorophores, $a = 52$ Å (vertical line in C).

consistent across several experimental conditions: the ADNFLE mutation is in either the $\alpha 4$ or the $\beta 2$ subunit, the fluorescent groups are in either the mutant or nonmutant subunit, the fluorescent control groups are in either the $\alpha 4$ or the $\beta 2$ subunits, and the subunit cDNAs are transfected at roughly equal levels or with excess $\beta 2$ cDNA. Thus, we can rule out effects on expression or assembly caused by the subunit carrying the mutation, by the type of fluorescent moiety (YFP versus CFP), or by its presence in a particular subunit.

Nicotine Counteracts the Bias toward $(\alpha 4)_3(\beta 2)_2$ of ADNFLE Receptors. Effects of long-term nicotine administration on nAChR subunit stoichiometry have been studied previously by several groups (Nelson et al., 2003; Moroni et al., 2006). These studies showed that exposure to nicotine preferentially up-regulates a high-sensitivity receptor population. For WT receptors, this population is usually assigned to the $(\alpha 4)_2(\beta 2)_3$ stoichiometry. We sought to determine whether incubation with nicotine shifts ADNFLE receptors toward the $(\alpha 4)_2(\beta 2)_3$ stoichiometry, despite the bias toward the opposite stoichiometry.

We first describe experiments with WT fluorescent receptors (Fig. 4A). Incubation in nicotine produced a significant decrease or increase in FRET efficiency when the XFP probes were in the $\alpha 4$ or $\beta 2$ subunits, respectively. This indicates that, as expected, incubation in nicotine shifts the receptor

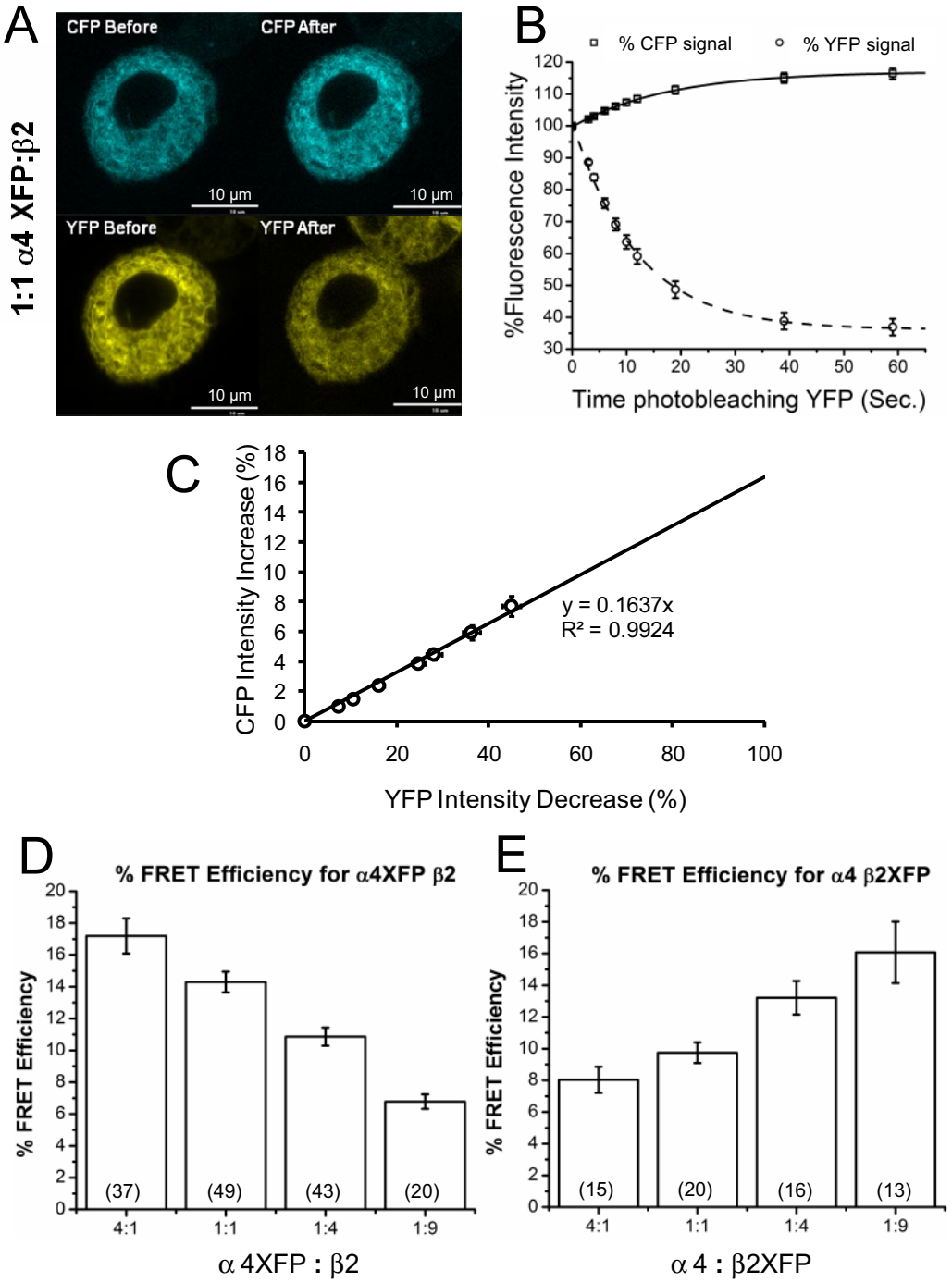

Fig. 2. Spectral images acquired before and after YFP bleaching were unmixed to calculate percent increase and decrease in CFP and YFP fluorescence intensities, respectively. A, representative unmixed images of a single N2a cell expressing 1:1 transfection ratio of $\alpha 4$XFP:$\beta 2$ cDNAs before and after photobleaching of the YFP fluorophore. B, time course of changes in CFP and YFP fluorescence intensity. C, scatter plot of CFP intensity increase versus YFP intensity decrease. This is extrapolated to 100% on the x-axis for the calculation of FRET efficiency (eq. 1). D and E, FRET efficiencies measured for transfections with forced stoichiometries. D, increased $\beta 2$ cDNA concentration during transfection with the $\alpha 4$XFP results in a decrease in percentage FRET efficiency. E, increased $\beta 2$XFP cDNA concentration during transfection with $\alpha 4$ results in an increase in percentage FRET efficiency.

population toward the $(\alpha4)_2(\beta2)_3$ stoichiometry. Our studies with fluorescence intensity ratios of subunit stoichiometry (Table 1 and Supplementary Material) agree with these findings.

We next describe analogous experiments with an ADFLE mutation, $\beta2$ V287L (Fig. 4B). In cells transfected with $\alpha4$ and $\beta2$ V287L XFP subunits, FRET efficiency was significantly higher after incubation in nicotine compared with control cells that were not exposed to nicotine. Likewise, cells transfected with $\alpha4$XFP $\beta2$ V287L and treated with nicotine showed lower FRET efficiency than unexposed cells. This result suggests a shift in stoichiometry toward $(\alpha4)_2(\beta2)_3$ in the presence of nicotine, partially or completely counteracting the shift produced by the ADNFLE mutant alone toward the $(\alpha4)_3(\beta2)_2$ population. The observed change in FRET efficiency in the presence of nicotine from cells transfected with $\alpha4$XFP and $\beta2$ V287L subunit was sufficient to bring the average values back to WT levels; this indicates that cells carrying an ADNFLE mutation in the presence of nicotine had subunit stoichiometry similar to that of the wild-type controls. The nicotine-induced shift was greater when the $\beta2$ V287L subunits were tagged with fluorescent proteins. In these cases, the effect of nicotine was dominant, and the average FRET efficiencies obtained from cells transfected with $\alpha4\beta2$XFP and $\alpha4\beta2$(V287L)XFP in the presence of nicotine did not differ significantly.

ADNFLE Mutations Bias toward $(\alpha4)_3(\beta2)_2$: Sensitized Emission Assays. We also analyzed the ADNFLE mutations $\beta2$ V287L and $\alpha4$ S248F, and the effects of long-term nicotine exposure, using pixel-resolved sensitized emission FRET measurements as described under *Materials and Methods* (Figs. 5 and 6). Sensitized emission measurements have the advantages of 1) speed, requiring only a few seconds, 2) greater resolution, allowing pixel-by-pixel measurements, and 3) nondestructive readout, allowing for repeated measurement on a given cell. However, sensitized emission measurements require greater attention to corrections for spectral unmixing and bleedthrough. Results obtained with the sensitized emission method agreed well with our DRAP results under the same conditions. Cells transfected with fluorescently tagged $\beta2$ V287L ADNFLE mutant subunits showed a significant 1.3-fold decrease in the mean FRET efficiency versus fluorescent non-ADNFLE subunits (Fig. 5, A, B, and G). On the other hand, we detected a significant 1.4-fold higher mean FRET efficiency from cells transfected with $\alpha4$XFP and $\beta2$V287L compared with the control cells transfected with WT subunits (Fig. 5, D, E, and

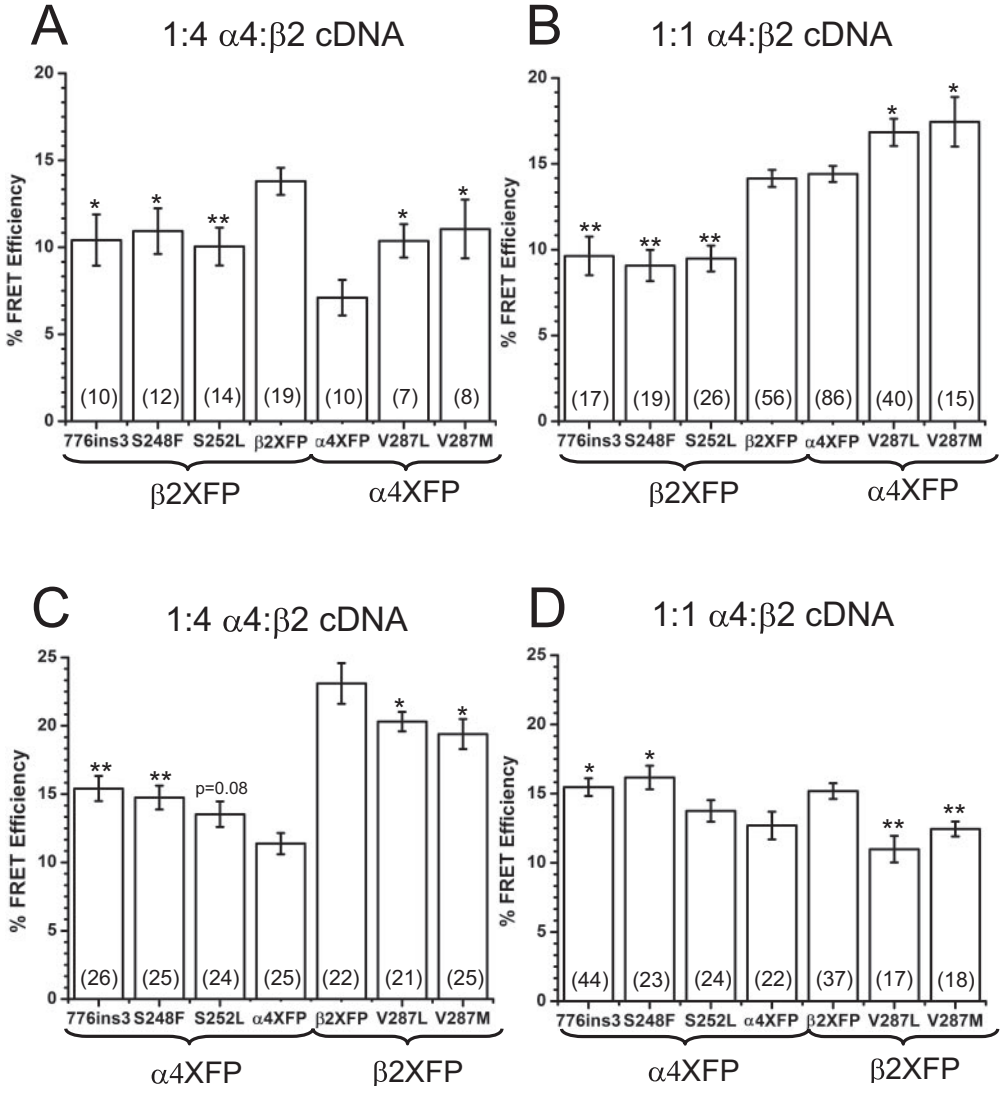

Fig. 3. ADNFLE mutations bias the $\alpha4\beta2$ receptor population toward the $(\alpha4)_3(\beta2)_2$ stoichiometry. A and B show FRET efficiency values measured by the DRAP method for five nonfluorescent ADNFLE mutant subunits transfected into N2a cells with the fluorescent WT complementary subunits ($\alpha4$XFP or $\beta2$XFP, where XFP denotes a 1:1 mixture of the CFP and YFP subunits). A, 1:4 cDNA ratio of $\alpha4$ to $\beta2$ subunits was transfected. B, 1:1 cDNA ratio of $\alpha4$ to $\beta2$ subunits was transfected. C and D show FRET efficiency values measured by the DRAP method for five fluorescent ADNFLE mutant subunits ($\alpha4$XFP or $\beta2$XFP, where XFP denotes a 1:1 mixture of the CFP and YFP ADNFLE subunits), transfected into N2a cells with the nonfluorescent WT complementary subunits. C, 1:4 cDNA ratio of $\alpha4$ to $\beta2$ subunits was transfected. D, 1:1 cDNA ratio of $\alpha4$ to $\beta2$ subunits was transfected. Data show mean ± S.E.M. (# of cells given in each bar). Significance was tested with unpaired two-tailed t test; *, $p \leq 0.05$; **, $p \leq 0.01$.

G). Both of these results imply a shift toward the $(\alpha4)_3(\beta2)_2$ stoichiometry.

Upon incubation of these cells with 1 μM nicotine for 48 h, the mean $\beta2$ intersubunit FRET efficiency increased to a level even higher than the control cells transfected with nonmutant fluorescent subunits (Fig. 5, C and G). Exposure to 1 μM nicotine for 48 h resulted in a decrease in the observed $\alpha4$ intersubunit FRET efficiency, in this case completely back to WT levels (Fig. 5, F and G). Both of these results showed that incubation in nicotine produces at least a reverse in the shifted stoichiometry that results from the ADNFLE mutation.

We also asked whether nicotine shifted the stoichiometry toward $(\alpha4)_2(\beta2)_3$ for the $\alpha4$ S248F mutation (Fig. 6). Experiments were performed with $\alpha4$ subunits carrying both the S248F mutation and XFP moieties. We found that incubation in nicotine (1 μM, 48 h) shifted the population toward the $(\alpha4)_2(\beta2)_3$ stoichiometry. Thus for the two ADNFLE mutations tested (one in the $\alpha4$ subunit, one in the $\beta2$ subunit), nicotine seems to partially or completely counteract the mutation-induced bias toward the $(\alpha4)_3(\beta2)_2$ stoichiometry.

FIRs Agree with FRET Measurements. We have also employed a FIR analysis (Staruschenko et al., 2005) to determine the stoichiometry of $\alpha4\beta2$ nAChRs using the same transfection conditions studied in the previous sections. Because the FIR measurements have not been extended to ADNFLE mutations, the method and data are presented briefly here and more fully in Supplementary material, including Supplementary Fig. 1. Summarizing the FIR procedure, we conducted two parallel experiments under identical conditions: α4CFP-β2YFP and α4YFP-β2CFP. These fluorescence data allow one to eliminate the differences in the efficiency of the optical systems for the two fluorophores used in these experiments. Thus, we acquired measurements of the actual ratio between $\alpha4$ and $\beta2$ subunits. The data confirmed that changing the ratio of $\alpha4$ to $\beta2$ cDNA governs the ratio of expressed subunits in assembled receptors; and the measured subunit ratios agreed acceptably with the measurements from FRET (Table 1). In other assays, we also detect that nicotine incubation produces the expected increase in the fraction of $(\alpha4)_2(\beta2)_3$ receptors (Table 1).

Overall Summary of Stoichiometric Differences Produced by ADNFLE Mutations and by Nicotine. We summarize the data on comparative stoichiometry from DRAP-FRET, pixel-based FRET, and FIR measurements exemplified in the figures. These data were gathered for the various subunit transfection ratios, various mutants, and various labeling strategies and were analyzed by the relation in Fig. 1D or by supplementary eqs. 12 and 13, as appropriate. In each experiment, ADNFLE and WT receptors were compared. The percentage of $(\alpha4)_3(\beta2)_2$ receptors is 1.2 times as great for ADNFLE receptors as for WT receptors (at least 12 experiments); the ratio was >1 in all experiments.

We also summarize the effects of nicotine; in each case, the experiment compared incubation in nicotine versus saline. The percentage of $(\alpha4)_3(\beta2)_2$ ADNFLE receptors is 0.8 times as great after nicotine incubation as after saline incubation (at least five experiments; the ratio was <1 in all cases).

Discussion

This study's most important conclusions are that ADNFLE may arise from defective regulation of nAChR subunit stoichiometry in an intracellular compartment(s) and that nicotine exposure reverses this defective stoichiometry. The internal consistency of the experiments rules out several alternative explanations. The bias toward $(\alpha4)_3(\beta2)_2$ is measured 1) when fluorescent groups are in either the mutant or nonmutant subunit, 2) for all three known $\alpha4$ subunit M2 domain ADNFLE mutations as well as for the two known $\beta2$ subunit M2 domain mutations, and 3) whether the subunit cDNAs are transfected at roughly equal levels or with excess

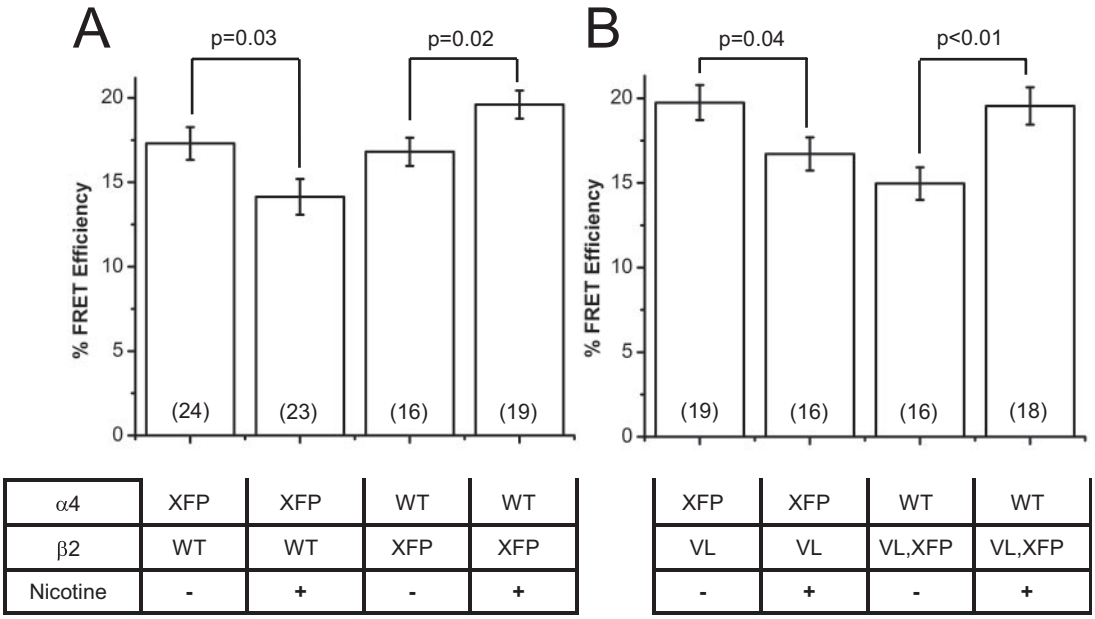

Fig. 4. Incubation in nicotine shifts both the WT receptor (**A**) and an ADNFLE receptor (B) toward the $(\alpha4)_2(\beta2)_3$ stoichiometry. FRET efficiency values were measured by the DRAP method. A, FRET efficiency measured for N2a cells transfected with 1:1 cDNA ratio of $\alpha4$XFP:$\beta2$ or $\alpha4$:$\beta2$XFP in the presence or absence of nicotine. B, FRET efficiency calculations for the N2a cells transfected with 1:1 cDNA ratio of $\alpha4$:$\beta2$ (V287L)XFP or $\alpha4$XFP:$\beta2$(V287L) in the presence or absence of nicotine. Data show mean ± S.E.M. (number of cells given in each bar).

β2 cDNA. The conclusions are supported by two substantially different FRET measurements (DRAP and sensitized emission), and FIR measurements also confirm the dependence of stoichiometry on transfection ratio. Thus, we have confidence that the conclusions do not arise from variations in expression or assembly caused by the fluorescent moiety, by YFP versus CFP, etc. Changes observed in all five cases show that the ADNFLE mutations produce an increment of 10 to 20% in the percentage of receptors with the $(\alpha4)_3(\beta2)_2$ stoichiometry.

ADNFLE: A Disease of nAChR Stoichiometry. As noted in the Introduction, the α4β2 nAChRs exist at least in two different stoichiometries, and it has been suggested that left-shifted dose-response relations arise because ADNFLE receptors have altered subunit stoichiometry. The present data strongly support this suggestion. We have used the terms high and low sensitivity to refer only to WT receptors, because it is possible that the higher sensitivity stoichiometry for ADNFLE receptors is $(\alpha4)_3(\beta2)_2$. The $(\alpha4)_3(\beta2)_2$ stoichiometry is the more sensitive form of the α4L9′T-β2 receptor (Moroni et al., 2006), and our unpublished data lead to the same conclusion for the α4L9′S-β2 and α4L9′A-β2 receptors, which produce an ADNFLE-like phenotype in knock-in mice (Fonck et al., 2003, 2005). If we independently knew the dose-response relations (or at least their relative positions) for the two stoichiometries of ADNFLE mutants, we could

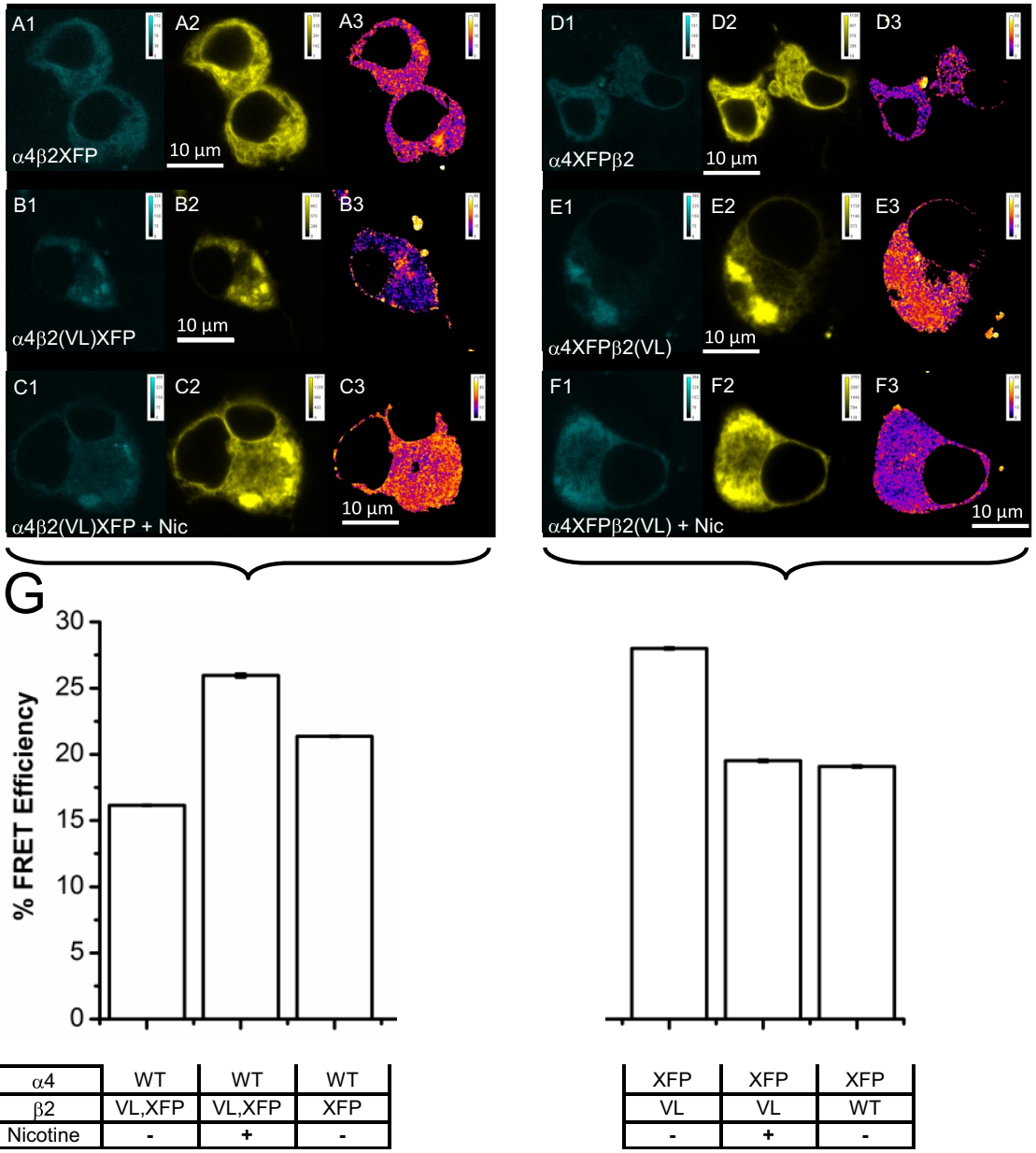

Fig. 5. Representative pixel-resolved sensitized emission FRET images for various conditions. Column 1 displays unmixed cell images in the CFP channel after 439 nm excitation; column 2 displays unmixed cell images in the YFP channel after 514-nm excitation; column 3 displays the percentage FRET efficiency images. Nicotine was present at 1 μM for 48 h where indicated. Row A, WT α4 subunit plus β2XFP. Rows B and C, WT α4 subunit plus β2(V287L)XFP. B, control incubation. C, incubation in nicotine. Row D, α4XFP plus WT β2. Rows E and F, α4XFP subunit plus β2V287L. E, control incubation. F, incubation in nicotine. G, average FRET efficiencies. Each column gives average overall pixels for 20 to 25 cells in each case. The S.E.M. is smaller than the width of the line in all cases. Data show mean ± S.E.M. (number of cells given in each bar). The S.E.M. (approximately the size of the lines delimiting the boxes) are smaller than in DRAP experiments, because S.E.M. is calculated on the basis of pixel numbers.

employ agonist-induced conductances to infer the relative surface stoichiometry of the ADNFLE mutations. However, the ADNFLE mutations probably have more subtle gating effects than the α4L9′T, L9′S, and L9′A mutations, vitiating assumptions about the relative sensitivities; at present, biochemical or fluorescence-based procedures lack the sensitivity to provide this information for the surface membrane compartment.

The internal consistency of the experiments argues against the possibility that our conclusions about altered stoichiometry, and about the effects of nicotine on this stoichiometry, derive artifactually from the presence of partially assembled "dead end" nAChRs (Kuryatov et al., 2005, 2008). In addition, the N2a expression system produces considerably lower levels of transfected membrane protein than do HEK293T cells, which produce appreciable numbers of dead-end nAChRs. However, we cannot rule out the possibility that partially assembled receptors produce some of the fluorescence.

How subunit dysregulation underlies the pathophysiology of ADNFLE is not known. Despite the left-shifted dose-response relations, in mammalian cells ADNFLE mutations produce rather low maximal ACh sensitivity or surface receptor levels (Kuryatov et al., 2005); and synaptosomes isolated from ADNFLE or ADNFLE-related knock-in mice gen-

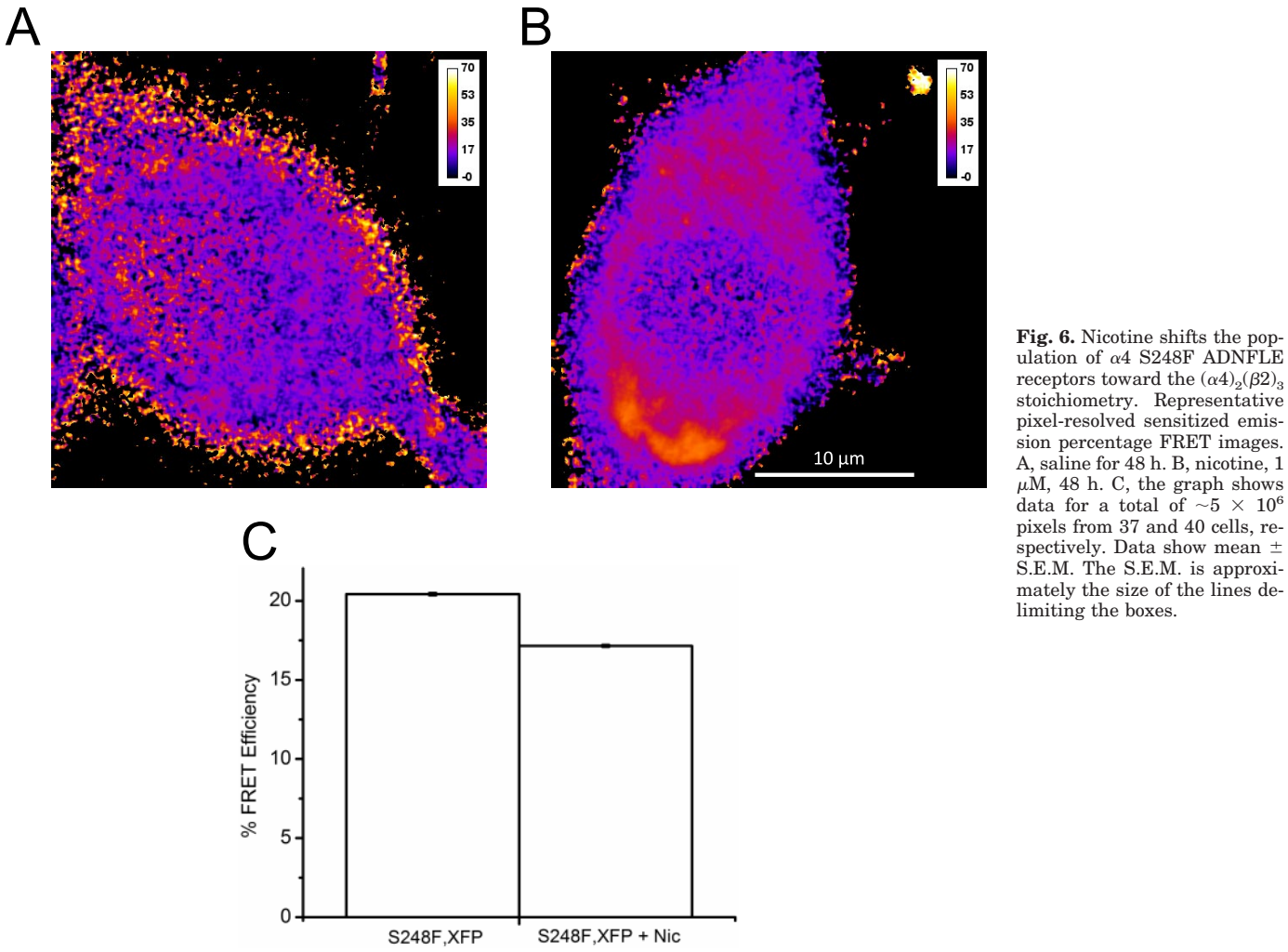

Fig. 6. Nicotine shifts the population of α4 S248F ADNFLE receptors toward the $(\alpha4)_2(\beta2)_3$ stoichiometry. Representative pixel-resolved sensitized emission percentage FRET images. A, saline for 48 h. B, nicotine, 1 μM, 48 h. C, the graph shows data for a total of ~5 × 10^6 pixels from 37 and 40 cells, respectively. Data show mean ± S.E.M. The S.E.M. is approximately the size of the lines delimiting the boxes.

TABLE 1

Percentage of $(\alpha4)_3(\beta2)_2$ for WT nAChRs observed under various conditions in this study and a previous study

FIR and FRET efficiency measurements were used to determine the subunit stoichiometry from cells transfected with various ratios of subunit cDNA and exposed to nicotine or low incubation temperatures. FRET measurements for WT subunits are derived from the experiment shown in Figure 2, C and D; FIR measurements are from the experiment shown in Supplementary Fig. 1. Data for incubation at 30°C are not shown. Results are compared to reported values.

	α4:β2					
	4:1	1:1	1:4	1:9	1:1	
					Nicotine	30°C
FIR	100	83	45	13	73	N.D.
FRET	94 ± 7	75 ± 3.5	52 ± 3	28 ± 3	61 ± 6	55 ± 6
Reported[a]	N.R.	82	43 ± 4	N.R.	68 ± 5	67 ± 6

N.R., not reported; N.D., not determined in the present experiments.
[a] Nelson et al. (2003).

erally show reduced function and reduced receptor numbers (Fonck et al., 2003, 2005; Teper et al., 2007; J. Xu, D. C. Laverty, C. Fonck, M. J. Marks, G. Dziewczapolski, B. N. Cohen, Y. Zhu, S. R. Grady, S. Panda, A. C. Collins, H. A. Lester, and S. F. Heinemann, unpublished data). These may be important clues for the pathophysiology of ADNFLE. Data are beginning to appear about functional effects of auxiliary subunits in nAChRs (Kuryatov et al., 2008), but, as noted above, we cannot yet address the important pathophysiological question of whether the altered intracellular stoichiometry of the intracellular receptors leads to similarly altered stoichiometry of surface receptors. Also, we still have an incomplete picture of the relation between stoichiometry and surface expression in various cellular regions (dendrites, soma, axons, and axon terminals). Because the seizures occur at night when the endogenous ACh levels are low, the seizures may be initiated by an imbalance between inhibitory and excitatory synaptic transmission (Rodrigues-Pinguet et al., 2005; Klaassen et al., 2006). Perhaps other epilepsies linked to Cys-loop receptors also arise from altered subunit stoichiometry (Wimmer et al., 2009).

Nicotine Effects. Long-term agonist or antagonist treatment is often associated with the functional and/or numerical up-regulation of $\alpha4\beta2$ nAChRs. Therefore, it has also been natural to suggest that repeated or long-term exposure to nicotine favors the high-sensitivity $(\alpha4)_2(\beta2)_3$ stoichiometry (Nelson et al., 2003; Sallette et al., 2005; Nashmi and Lester, 2007). The control experiments with WT subunits did extend the previous reports showing that long-term exposure to nicotine results in an up-regulation of the $(\alpha4)_2(\beta2)_3$ configuration (Nelson et al., 2003) (FRET, Figs. 4A and 5; FIR, Table 1).

The effect of nicotine incubation on the $\alpha4\beta2$V287L (Figs. 4B and 5G) and $\alpha4$S248F (Fig. 6) nAChRs was similar to the effect on WT: exposure to nicotine favors the $(\alpha4)_2(\beta2)_3$ configuration. We conclude that effects of nicotine are dominant over the effects of the ADNFLE mutation, because nicotine can revert the subunit stoichiometry to nearly WT ratios. This nicotine-induced shift back to the presumably nonpathogenic WT stoichiometry may help explain how nicotine patches or smoking suppress seizure phenotype in patients with ADNFLE (Willoughby et al., 2003; Brodtkorb and Picard, 2006).

Pharmacological Chaperoning by Nicotine. Because the present study emphasizes intracellular receptors, it supports recent suggestions that nicotine is an intracellular pharmacological chaperone of WT $\alpha4\beta2$ nAChRs (Kuryatov et al., 2005; Sallette et al., 2005; Vallejo et al., 2005; Nashmi and Lester, 2007), stabilizing the $(\alpha4)_2(\beta2)_3$ stoichiometry (Kuryatov et al., 2005) of this multisubunit membrane protein (Wiseman et al., 2007; Balch et al., 2008). Evidently, the ADNFLE mutations change the relative stability of the assembled $(\alpha4)_2(\beta2)_3$ and $(\alpha4)_3(\beta2)_2$ conformations, either destabilizing the former or stabilizing the latter. This is slightly surprising, because most of our knowledge about intersubunit contacts lead us to emphasize the N-terminal binding rather than the M2 helices as major determinants of assembly. Nonetheless, the data show that the apparent chaperone effect of nicotine also stabilizes the $(\alpha4)_2(\beta2)_3$ stoichiometry of the ADNFLE mutant subunits, similar to its action on WT subunits. We are interested in conducting FRET experiments to study more details of pharmacological chaperoning by nicotine, including time-resolved measurements and subcellular localization.

Fluorescence-Based Measurements of Subunit Stoichiometry. We believe that this study shows the first fluorescence-based distinction between two and three subunits in a pentameric Cys-loop receptor, although the FRET method depends heavily on theories developed for the pentameric MscL channel (Corry et al., 2005, 2006; Corry and Jayatilaka, 2008). Therefore, this report quantitatively extends previous studies of nAChR subunit stoichiometry using fluorescently tagged nAChR subunits in HEK293T cells (Nashmi et al., 2003), in transfected cultured neurons (Nashmi et al., 2003; Khakh et al., 2005; Drenan et al., 2008), in knock-in mice (Nashmi and Lester, 2007; Nashmi et al., 2007), and in cultured N2a cells (Drenan et al., 2008). In previous studies, the work of our own laboratory and several others distinguished between 1 and $\geq$2 subunits. FRET theory, combined with the known geometrical and biological constraints in pentameric $\alpha4\beta2$ receptor populations, suggested that FRET among $\alpha4$ subunits, or among $\beta2$ subunits, is a sensitive procedure to detect more subtle stoichiometric relations. The explicit theory presented in the *Appendix* and in Fig. 1 (Corry et al., 2005, 2006; Corry and Jayatilaka, 2008) leads to a linear relation between the FRET efficiency and the percentage of receptor populations carrying two versus three fluorescently tagged subunits (Fig. 1D). The data show that FRET efficiency for $(\alpha4\text{XFP})_3(\beta2)_2$ is indeed significantly higher than for $(\alpha4\text{XFP})_2(\beta2)_3$ and that cells expressing mostly $(\alpha4)_2(\beta2\text{XFP})_3$ have higher FRET efficiency than the cells expressing mostly $(\alpha4)_3(\beta2\text{XFP})_2$ receptors, as predicted (Fig. 2, C and D). These conclusions are supported by a rather different type of fluorescence analysis, FIR (Zheng and Zagotta, 2004) (Supplementary Fig. 1). Table 1 summarizes how these results generally agree with the previously reported shifts observed by metabolic labeling with [^{35}S]methionine and biphasic dose response curves.

It is noteworthy that one can perform these fluorescence-based measurements using live cultures. Pixel-by-pixel sensitized emission measurements are conducted with minimal destruction of the fluorophores (Fig. 5 and 6), in principle allowing repeated observations on a single cell. Using this information, one can determine the changes in the subunit stoichiometry due to ADNFLE mutations, environmental conditions (such as incubation temperature), or due to chaperoning by ligand (nicotine) interaction. The addictive properties of nicotine are thought to depend partially on these ligand-induced changes in subunit number and stoichiometry. The (inadvertent) therapeutic effects of smoking in ADNFLE (analyzed in this article), and perhaps the inverse correlation between smoking and Parkinson's disease, arise from similar changes (Nashmi et al., 2007). Therefore, we expect that fluorescence of nAChR subunits will become a useful procedure for drug discovery.

Appendix

This *Appendix* presents the theory of FRET measurements to determine subunit stoichiometry. The analysis uses several simplifying geometric assumptions.

1. In a functional $\alpha4\beta2$ receptor, there are at least two agonist binding sites at the α-β subunit interfaces (these are polar-

ized, requiring particular faces of each subunit; see assumption 2 below). Therefore, in the $(\alpha4)_2(\beta2)_3$ stoichiometry, the two $\alpha4$ subunits are nonadjacent, and in the $(\alpha4)_3(\beta2)_2$ stoichiometry, the two $\beta2$ subunits are nonadjacent.

2. In the diagrams of Fig. 1, A and B, the receptor is viewed from the extracellular faces, so that the β subunit is adjacent, in the clockwise direction, to the α subunit.
3. Although the intracellular domain of the $\alpha4$ subunit has roughly twice as many amino acids as that of the $\beta2$ subunit, the fluorophores are positioned in an equilateral pentagonal structure.
4. All $\alpha4$ subunits are radially equivalent, and all $\beta2$ subunits are radially equivalent.
5. Because YFP and CFP differ by only nine amino acids, YFP- and CFP-tagged subunits are synthesized with equal efficiency and assemble randomly within receptor pentamers. The expected results are rather insensitive to departures from this assumption by even 2-fold.
6. Again, because YFP and CFP differ only subtly, the structure of an $\alpha4$CFP subunit is the same as $\alpha4$YFP; in addition, a $\beta2$CFP subunit has the same structure as a $\beta2$YFP subunit.
7. In a rigorous analysis, the dipole orientation factor κ^2 differs between adjacent and nonadjacent subunit pairs. Analysis shows that, in general, the ratio κ^2 (nonadjacent subunits)/κ^2 (adjacent subunits) lies between 1 and 2; a full prediction requires knowledge of the dipole orientation, which we do not know (Corry et al., 2006). We assume that this ratio always equals 1.

In such a pentameric receptor, there are two possible distances between fluorophores: a, the side length between adjacent subunits, and b, the diagonal between nonadjacent subunits (Fig. 1A). These are given by:

$$b/a = (1 + \sqrt{5}/2) = 1.618 \tag{4}$$

Thus the efficiencies of energy transfer within an isolated pentameric receptor can be calculated analytically depending on the position of the donor and the acceptor. Most measurements in this study use the simple case in which the fluorophores are present in all $\alpha4$ subunits, but none of the $\beta2$ subunits or vice versa. To simplify the terminology, we explicitly analyze the case for fluorescent $\alpha4$ subunits; the results apply, of course, to the fluorescent $\beta2$ case as well.

For the $(\alpha4)_2(\beta2)_3$ stoichiometry, the fluorophore separation is the nonadjacent value b. Therefore, the FRET efficiency is

$$E_b\left(\frac{(R_0/b)^6}{1 + (R_0/b)^6}\right); \tag{5}$$

(where R_0 is the Förster distance of the FRET pair) and the statistical factors are rather simple: 50% of the molecules have heterogeneous fluorophores and therefore display FRET (our methods do not determine homo-FRET) (Fig. 1B).

The situation is more complex for the $(\alpha4)_3(\beta2)_2$ pentamer (Fig. 1B). For instance, the FRET efficiency for one donor, nonadjacent to two acceptors, is

$$E_1\left(\frac{2(R_0/b)^6}{1 + 2(R_0/b)^6}\right); \tag{6}$$

for one donor, adjacent and nonadjacent to two acceptors, E is

$$E_2 = \left(\frac{R_0^6\left(\frac{1}{a^6} + \frac{1}{b^6}\right)}{1 + R_0^6\left(\frac{1}{a^6} + \frac{1}{b^6}\right)}\right); \tag{7}$$

for two donors, both nonadjacent to a single acceptor, E is simply

$$E_3 = E_b. \tag{8}$$

For two donors, one adjacent and the other nonadjacent to a single acceptor,

$$E_4 = \frac{1}{2}\left(\frac{\left(\frac{R_0}{a}\right)^6}{1 + \left(\frac{R_0}{a}\right)^6} + \frac{\left(\frac{R_0}{b}\right)^6}{1 + \left(\frac{R_0}{b}\right)^6}\right). \tag{9}$$

The total FRET efficiency is now the weighted sum of E for a particular configuration, times the probability that the configuration occurs. These statistical factors are given in Fig. 1B (Corry et al., 2005).

These calculations lead to an expected series of FRET efficiencies as a function of the distance a between adjacent fluorophores (Fig. 1C). Note that the FRET efficiency does not approach 1 as a approaches 0, because in some pentamers, all tagged subunits carry either donors or acceptors, in which case our measurement cannot detect FRET. Because 25% of the assembled receptors are composed of three tagged subunits and 50% of the receptors carrying two tagged subunits lack FRET partners, the FRET efficiency curves in Fig. 1C intersect the y-axis between 75 and 50%.

The final step in the theoretical analysis (Fig. 1D) is to assume a reasonable value for the distance a between adjacent fluorophores. In the absence of structural data for the intracellular loop of any Cys-loop receptor, this must be a guess. We assume a value of $a = 52$ Å, which is also consistent with structural studies of the neuromuscular receptor (Unwin, 2005). However, any distance within ~40 Å and ~60 Å would generate the same conclusion: FRET efficiencies are quite measurable (10–40%) if all the pentamers have the $(\alpha4)_3(\beta2)_2$ stoichiometry. The solid line in Fig. 1D shows that as the percentage of $(\alpha4)_3(\beta2)_2$ decreases to zero (with a complementary increase of $(\alpha4)_2(\beta2)_3$), the theoretical FRET efficiency drops by ~10 fold.

For any chosen value of a, the theoretical FRET efficiency depends linearly on the percentage of $(\alpha4)_3(\beta2)_2$ stoichiometry. For $a = 45$ Å, the maximum and minimum FRET values are 29.3 and 4.8%, respectively; for $a = 60$ Å, these extremes are 10.6 and 0.9%, respectively.

Acknowledgments

We thank Princess Imoukhuede, Rigo Pantoja, Rahul Srinivasan, Larry Wade, and Ben Corry (University of Western Australia) for discussion and Jeff Larsen (Nikon) for much technical help.

References

Balch WE, Morimoto RI, Dillin A, and Kelly JW (2008) Adapting proteostasis for disease intervention. *Science* **319:**916–919.

Benowitz NL, Kuyt F, and Jacob P 3rd (1982) Circadian blood nicotine concentrations during cigarette smoking. *Clin Pharmacol Ther* **32:**758–764.

Bertrand D, Picard F, Le Hellard S, Weiland S, Favre I, Phillips H, Bertrand S, Berkovic SF, Malafosse A, and Mulley J (2002) How mutations in the nAChRs can cause ADNFLE epilepsy. *Epilepsia* **43 (Suppl 5):**112–122.

Briggs CA, Gubbins EJ, Marks MJ, Putman CB, Thimmapaya R, Meyer MD, and

Surowy CS (2006) Untranslated region-dependent exclusive expression of high-sensitivity subforms of $\alpha4\beta2$ and $\alpha3\beta2$ nicotinic acetylcholine receptors. *Mol Pharmacol* **70:**227–240.

Brodtkorb E and Picard F (2006) Tobacco habits modulate autosomal dominant nocturnal frontal lobe epilepsy. *Epilepsy Behav* **9:**515–520.

Buisson B and Bertrand D (2001) Chronic exposure to nicotine up-regulates the human $\alpha4\beta2$ nicotinic acetylcholine receptor function. *J Neurosci* **21:**1819–1829.

Combi R, Dalprà L, Tenchini ML, and Ferini-Strambi L (2004) Autosomal dominant nocturnal frontal lobe epilepsy–a critical overview. *J Neurol* **251:**923–934.

Corry B and Jayatilaka D (2008) Simulation of structure, orientation, and energy transfer between AlexaFluor molecules attached to MscL. *Biophys J* **95:**2711–2721.

Corry B, Jayatilaka D, Martinac B, and Rigby P (2006) Determination of the orientational distribution and orientation factor for transfer between membrane-bound fluorophores using a confocal microscope. *Biophys J* **91:**1032–1045.

Corry B, Jayatilaka D, and Rigby P (2005) A flexible approach to the calculation of resonance energy transfer efficiency between multiple donors and acceptors in complex geometries. *Biophys J* **89:**3822–3836.

Derry CP, Davey M, Johns M, Kron K, Glencross D, Marini C, Scheffer IE, and Berkovic SF (2006) Distinguishing sleep disorders from seizures: diagnosing bumps in the night. *Arch Neurol* **63:**705–709.

Drenan RM, Nashmi R, Imoukhuede P, Just H, McKinney S, and Lester HA (2008) Subcellular trafficking, pentameric assembly, and subunit stoichiometry of neuronal nicotinic ACh receptors containing fluorescently labeled $\alpha6$ and $\beta3$ subunits. *Mol Pharmacol* **73:**27–41.

Elangovan M, Wallrabe H, Chen Y, Day RN, Barroso M, and Periasamy A (2003) Characterization of one- and two-photon excitation fluorescence resonance energy transfer microscopy. *Methods* **29:**58–73.

Feige JN, Sage D, Wahli W, Desvergne B, and Gelman L (2005) PixFRET, an ImageJ plug-in for FRET calculation that can accommodate variations in spectral bleedthroughs. *Microsc Res Tech* **68:**51–58.

Figl A, Viseshakul N, Shafaee N, Forsayeth J, and Cohen BN (1998) Two mutations linked to nocturnal frontal lobe epilepsy cause use-dependent potentiation of the nicotinic ACh response. *J Physiol* (*Lond*) **513:**655–670.

Fonck C, Cohen BN, Nashmi R, Whiteaker P, Wagenaar DA, Rodrigues-Pinguet N, Deshpande P, McKinney S, Kwoh S, Munoz J, et al. (2005) Novel seizure phenotype and sleep disruptions in knock-in mice with hypersensitive $\alpha4$ nicotinic receptors. *J Neurosci* **25:**11396–113411.

Fonck C, Nashmi R, Deshpande P, Damaj MI, Marks MJ, Riedel A, Schwarz J, Collins AC, Labarca C, and Lester HA (2003) Increased sensitivity to agonist-induced seizures, Straub tail, and hippocampal theta rhythm in knock-in mice carrying hypersensitive $\alpha4$ nicotinic receptors. *J Neurosci* **23:**2582–2590.

Herman ST, Walczak TS, and Bazil CW (2001) Distribution of partial seizures during the sleep-wake cycle: differences by seizure onset site. *Neurology* **56:**1453–1459.

Imoukhuede PI, Moss FJ, Michael DJ, Chow RH and Lester HA (2009) Ezrin mediates tethering of the γ-aminobutyric acid transporter GAT1 to actin filaments via a C-terminal PDZ-interacting domain. *Biophys J* doi: 10.1016/j.bpj.2008.11.070.

Khakh BS, Fisher JA, Nashmi R, Bowser DN, and Lester HA (2005) An angstrom scale interaction between plasma membrane ATP-gated P2X2 and $\alpha4\beta2$ nicotinic channels measured with FRET and TIRF microscopy. *J Neurosci* **25:**6911–6920.

Klaassen A, Glykys J, Maguire J, Labarca C, Mody I, and Boulter J (2006) Seizures and enhanced cortical GABAergic inhibition in two mouse models of human autosomal dominant nocturnal frontal lobe epilepsy. *Proc Natl Acad Sci U S A* **103:**19152–19157.

Kuryatov A, Luo J, Cooper J, and Lindstrom J (2005) Nicotine acts as a pharmacological chaperone to up-regulate human $\alpha4\beta2$ acetylcholine receptors. *Mol Pharmacol* **68:**1839–1851.

Kuryatov A, Onksen J, and Lindstrom J (2008) Roles of accessory subunits in $\alpha4\beta2\alpha5$ nicotinic receptors. *Mol Pharmacol* **74:**132–143.

Mansvelder HD and McGehee DS (2000) Long-term potentiation of excitatory inputs to brain reward areas by nicotine. *Neuron* **27:**349–357.

Moroni M, Zwart R, Sher E, Cassels BK, and Bermudez I (2006) $\alpha4\beta2$ nicotinic receptors with high and low acetylcholine sensitivity: pharmacology, stoichiometry, and sensitivity to long-term exposure to nicotine. *Mol Pharmacol* **70:**755–768.

Nashmi R, Dickinson ME, McKinney S, Jareb M, Labarca C, Fraser SE, and Lester HA (2003) Assembly of $\alpha4\beta2$ nicotinic acetylcholine receptors assessed with functional fluorescently labeled subunits: effects of localization, trafficking, and nicotine-induced up-regulation in clonal mammalian cells and in cultured midbrain neurons. *J Neurosci* **23:**11554–11567.

Nashmi R and Lester H (2007) Cell autonomy, receptor autonomy, and thermodynamics in nicotine receptor up-regulation. *Biochem Pharmacol* **74:**1145–1154.

Nashmi R, Xiao C, Deshpande P, McKinney S, Grady SR, Whiteaker P, Huang Q, McClure-Begley T, Lindstrom JM, Labarca C, et al. (2007) Chronic nicotine cell specifically up-regulates functional $\alpha4^*$ nicotinic receptors: basis for both tolerance in midbrain and enhanced long-term potentiation in perforant path. *J Neurosci* **27:**8202–8218.

Nelson ME, Kuryatov A, Choi CH, Zhou Y, and Lindstrom J (2003) Alternate stoichiometries of $\alpha4\beta2$ nicotinic acetylcholine receptors. *Mol Pharmacol* **63:**332–341.

Oldani A, Zucconi M, Asselta R, Modugno M, Bonati MT, Dalprà L, Malcovati M, Tenchini ML, Smirne S, and Ferini-Strambi L (1998) Autosomal dominant nocturnal frontal lobe epilepsy. A video-polysomnographic and genetic appraisal of 40 patients and delineation of the epileptic syndrome. *Brain* **121:**205–223.

Partridge JG, Apparsundaram S, Gerhardt GA, Ronesi J, and Lovinger DM (2002) Nicotinic acetylcholine receptors interact with dopamine in induction of striatal long-term depression. *J Neurosci* **22:**2541–2549.

Provini F, Plazzi G, Tinuper P, Vandi S, Lugaresi E, and Montagna P (1999) Nocturnal frontal lobe epilepsy. A clinical and polygraphic overview of 100 consecutive cases. *Brain* **122:**1017–1031.

Rodrigues-Pinguet N, Jia L, Li M, Figl A, Klaassen A, Truong A, Lester HA, and Cohen BN (2003) Five ADNFLE mutations reduce the Ca^{2+} dependence of the $\alpha4\beta2$ acetylcholine response. *J Physiol* **550:**11–26.

Rodrigues-Pinguet NO, Pinguet TJ, Figl A, Lester HA, and Cohen BN (2005) Mutations linked to autosomal dominant nocturnal frontal lobe epilepsy affect allosteric Ca^{2+} activation of the $\alpha4\beta2$ nicotinic acetylcholine receptor. *Mol Pharmacol* **68:**487–501.

Ryvlin P, Rheims S, and Risse G (2006) Nocturnal frontal lobe epilepsy. *Epilepsia* **47 (Suppl 2):**83–86.

Sallette J, Pons S, Devillers-Thiery A, Soudant M, Prado de Carvalho L, Changeux JP, and Corringer PJ (2005) Nicotine up-regulates its own receptors through enhanced intracellular maturation. *Neuron* **46:**595–607.

Scheffer IE, Bhatia KP, Lopes-Cendes I, Fish DR, Marsden CD, Andermann E, Andermann F, Desbiens R, Keene D, and Cendes F (1995) Autosomal dominant nocturnal frontal lobe epilepsy. A distinctive clinical disorder. *Brain* **118:**61–73.

Staruschenko A, Adams E, Booth RE, and Stockand JD (2005) Epithelial Na^+ channel subunit stoichiometry. *Biophys J* **88:**3966–3975.

Steinlein OK, Magnusson A, Stoodt J, Bertrand S, Weiland S, Berkovic SF, Nakken KO, Propping P, and Bertrand D (1997) An insertion mutation of the CHRNA4 gene in a family with autosomal dominant nocturnal frontal lobe epilepsy. *Hum Mol Genet* **6:**943–947.

Teper Y, Whyte D, Cahir E, Lester HA, Grady SR, Marks MJ, Cohen BN, Fonck C, McClure-Begley T, McIntosh JM, et al. (2007) Nicotine-induced dystonic arousal complex in a mouse line harboring a human autosomal dominant nocturnal frontal lobe epilepsy mutation. *J Neurosci* **27:**10128–10142.

Unwin N (2005) Refined structure of the nicotinic acetylcholine receptor at 4Å resolution. *J Mol Biol* **346:**967–989.

Vallejo YF, Buisson B, Bertrand D, and Green WN (2005) Chronic nicotine exposure up-regulates nicotinic receptors by a novel mechanism. *J Neurosci* **25:**5563–5572.

Willoughby JO, Pope KJ, and Eaton V (2003) Nicotine as an antiepileptic agent in ADNFLE: an N-of-one study. *Epilepsia* **44:**1238–1240.

Wimmer VC, Lester HA, and Petrou S (2009) Ion channel mutations in familial epilepsy, in *Encyclopedia of Basic Epilepsy Research* (Schwartzkroin PA ed) in press, Academic Press, London.

Wiseman RL, Powers ET, Buxbaum JN, Kelly JW, and Balch WE (2007) An adaptable standard for protein export from the endoplasmic reticulum. *Cell* **131:**809–821.

Wong JY, Ross SA, McColl C, Massalas JS, Powney E, Finkelstein DI, Clark M, Horne MK, Berkovic SF, and Drago J (2002) Proconvulsant-induced seizures in $\alpha4$ nicotinic acetylcholine receptor subunit knockout mice. *Neuropharmacology* **43:**55–64.

Zheng J and Zagotta WN (2004) Stoichiometry and assembly of olfactory cyclic nucleotide-gated channels. *Neuron* **42:**411–421.

Zwart R, Broad LM, Xi Q, Lee M, Moroni M, Bermudez I, and Sher E (2006) 5-I A-85380 and TC-2559 differentially activate heterologously expressed $\alpha4\alpha\beta2$ nicotinic receptors. *Eur J Pharmacol* **539:**10–17.

Address correspondence to: Henry A. Lester, Division of Biology, MC 156-29, California Institute of Technology, Pasadena, CA 91125. E-mail: lester@caltech.edu